Int J Adv Manuf Technol (2017) 90:1023–1033
DOI 10.1007/s00170-016-9463-x

ORIGINAL ARTICLE

Signal processing and pattern recognition for surface roughness assessment in multiple sensor monitoring of robot-assisted polishing

Tiziana Segreto [1,2] · **Sara Karam** [1,2] · **Roberto Teti** [1,2]

Received: 31 May 2016 / Accepted: 6 September 2016 / Published online: 16 September 2016

Abstract Polishing processes have steadily evolved from largely manual operations to automated processes based on robotized systems. Sensor monitoring can be a viable solution for process control in order to achieve more accurate, robust, and reliable automated polishing operations. In this paper, an acoustic emission-, strain-, and current-based sensor-monitoring system was employed during robot-assisted polishing of steel bars for online assessment of workpiece surface roughness. Two feature extraction procedures, a conventional one based on statistics and an advanced one based on wavelet packet transform, were applied to the sensor signals detected during polishing. The extracted relevant features were utilized to construct different types of pattern feature vectors (basic and sensor fusion pattern vectors) to be fed to a neural network pattern recognition paradigm in order to make a decision on polished part surface roughness-level acceptability.

Keywords Polishing · Multiple sensor monitoring · Surface roughness · Feature extraction · Pattern recogniton · Neural networks

✉ Tiziana Segreto
tsegreto@unina.it

[1] Fraunhofer Joint Laboratory of Excellence on Advanced Production Technology (Fh-J_LEAPT Naples), Naples, Italy

[2] Department of Chemical, Materials and Industrial Production Engineering, University of Naples Federico II, Piazzale Tecchio 80, 80125 Naples, Italy

1 Introduction

A workpiece fabrication comprises of a series of manufacturing processes, casting, forming, machining, etc. To conclude fabrication, surface finishing is performed in order to smoothen surfaces until the required surface roughness is reached [1]. To date, one of the best-performing surface-finishing processes, capable to create mirror-like surfaces, is polishing [2], which is defined as the process of generating a surface smoother than the initial one [3].

Initially, polishing was a manual process performed by skilled human operators. Gradually, it is becoming an automated process [4] aiming at improving the polishing operation performance in terms of time reduction and quality assurance. Robot-assisted polishing (RAP) consists of a motorized arm that performs polishing on a given workpiece [5]. The motorized arm holds the polishing tool and displaces it back and forth, at a set speed, along a chosen stroke length on the workpiece surface to be polished. The polishing parameters are programmed by setting the main spindle rotational speed, the cutting speed, the cutting force, the stroke length, and the pulse rate.

In polishing, surface roughness is the quality parameter of interest consisting of the irregularity measurement in the surface that results from manufacturing process. Essentially, surface inspection methods are based on tactile methods that measure surface roughness through physical contact with the workpiece surface [6]. This direct inspection method necessitates the halting of the polishing operation to allow the measurement of the workpiece surface roughness.

Online process control is essential for the complete automation, performance, and quality improvement of manufacturing processes and can be implemented by employing innovative sensor-monitoring systems characterized by high robustness, reliability, reconfigurability, and intelligence [7–10].

The application of sensor monitoring for manufacturing processes, in particular for machining processes, has been of increasing interest of study and research over the past 30 years. The first detailed investigation of sensorial systems for tool wear estimation was published by Micheletti et al. [11] in 1976. Tönshoff et al. [12] disclosed the developments and trends of monitoring and control of cutting processes in 1988. Byrne et al. [7] compiled an accurate report on the state of the art of industrial application of cutting process of monitoring in 1995. Teti et al. [13] in 2010 promoted the recent advancements on advanced monitoring of machining operations. However, the results of these research activities indicated that the commercial monitoring systems were excessively specialized for the purposes of practical applications, and their employment in industry was limited. This was due to the fact that most of the commercial monitoring systems were based on the use of a single sensor.

A new focus of the research on sensor signals relates to fusion of sensory data obtained by combining homogeneous or heterogeneous sensory devices for enhanced process characterization [14, 15]. Many definitions for data fusion exist in literature. Historically, data fusion methods were developed primarily for military applications. Joint Directors of Laboratories [16] defines data fusion as a "multilevel, multifaceted process handling the automatic detection, association, correlation, estimation, and combination of data and information from several sources." In recent years, data fusion methods were applied in diverse areas such as signal processing, information theory, statistical evaluation, and artificial intelligence. In machining processes, sensory data fusion techniques were utilized for the following main purposes: tool state identification [17], process condition optimization [18], surface integrity evaluation [19], and machine tool state [20].

As regards polishing processes, there are few experimental studies on the implementation of multiple sensor monitoring and data fusion methods for process optimization and automation [21, 22]. Among them, the use of acoustic emission sensors has allowed the achievement of valuable results for the estimation of the process state [23–25].

This research work focuses on the development of a multiple sensor-monitoring process system for improved control and enhanced repeatability and predictability of a robot-assisted polishing process. For this purpose, an experimental campaign was carried out, using a RAP machine [26] to polish American Iron and Steel Institute (AISI) 52100 alloy steel bars by varying polishing conditions. Three diverse sensing units, acoustic emission (AE), strain, and current, were installed on the RAP machine for sensor signal detection. The following two feature extraction techniques were applied to the digitized sensor signals: a conventional one based on statistical analysis and an advanced one based on wavelet packet transform (WPT) [27, 28]. The relevant extracted statistical and WPT features were utilized to construct the following two kinds of pattern feature vectors: 5-element pattern feature vectors and 15-element sensor fusion pattern feature vectors. These vectors were used as input to a neural network (NN) pattern recognition paradigm [29, 30] to correlate the sensor signals to the measured surface roughness in order to make an online decision on the acceptability of the polished workpiece surface roughness.

2 Experimental procedure

2.1 Robot-assisted polishing machine

The RAP machine is a motorized arm that imitates the work and skills of polishers who are able to polish, following a series of operations, bringing the surface roughness level down to a mirror-like surface removing scratches and defects. The main objective behind creating and building the RAP machine is to overcome the time-consuming operational labor of hand polishing. Moreover, the RAP machine should be able to remove defects from previous machining processes and ensuring that the final surface has a roughness level adequate for the subsequent application.

The RAP machine, utilized in this paper, is composed of a main spindle and a polishing module (Fig. 1) [31]. The workpiece to be polished is chucked to the main spindle, which is driven by a direct-drive servomotor. This part of the RAP machine operates similarly to a turning lathe. The rotational speed of the chuck, and thus the mounted workpiece, is programmed. The polishing module combines a robot arm on which interchangeable polishing stones are mounted, a force sub-module, and a control module. The force sub-module applies a force orthogonal to the surface of the workpiece to be polished. While applying this force, the polishing stone pulsates along a defined stroke length.

As for the pulsation and rotation-driven tool module, the controlling parameters (pulse frequency or rotational speed) and non-conventional polishing parameters (cutting speed and

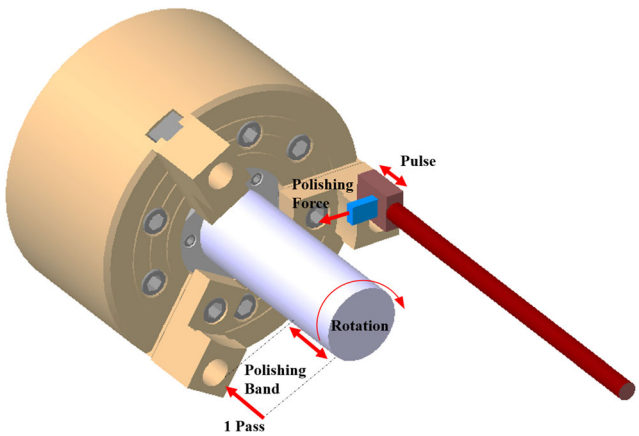

Fig. 1 Scheme of the RAP machine

feed rate) can be controlled by the RAP program, which is the control module of the RAP machine.

2.2 Experimental polishing tests

The experimental polishing test campaign was carried out within the activities of the EC FP7 Project Intelligent Fault Correction and self-Optimizing Manufacturing systems "IFaCOM" [32]. AISI 52100 alloy steel cylindrical bars (Ø 40 × 75 mm) (Fig. 2) were polished using a silicon carbide-polishing stone with no. 800 grit size.

The experimental setup used during the polishing tests was the following:

– Spindle speed 300 rpm
– Feed rate 5 mm/s
– Polishing force 1000 or 1800 g
– Pulse rate 500 pulses/min
– Stroke length 1 mm.

The polishing testing sessions were 6, each composed of 60 passes. Each testing session had an approximate duration of 15 min and 50 s. A pass is defined as the polished path that goes from one end of the desired length to be polished down to the other extremity.

During the six testing sessions, the full length of the alloy steel bar was polished over and over using different polishing force as shown below.

- 1800 g in the first session, 1 session × 60 passes = a total of 60 passes (from pass no 1 to no. 60)
- 1000 g in the second, third, and fourth sessions, 3 sessions × 60 passes = a total of 180 passes (from pass no. 61 to no. 240)
- 1800 g in the fifth and sixth sessions, 2 sessions × 60 passes = a total of 120 passes (from pass no. 241 to no. 360).

2.3 Multiple sensor-monitoring system

Three diverse sensing units were employed during the polishing tests, comprising (Fig. 3)

- AE sensor fixed on the tool holder. The AE signals were pre-amplified and high-pass filtered with a 50-kHz cutoff frequency. Then, the AE signals were digitized at a 1-MS/s sampling rate and finally undersampled at almost 131 kS/s.
- Strain gauge sensor mounted between the tool holder and the robot arm connection to measure the force generated during polishing. The strain signal was digitized at a 50-kS/s sampling rate and then undersampled at almost 16 kS/s.
- Current sensor mounted in the electrical cabinet of the machine providing signals related to the motor power absorbance. The current signal was digitized at a 50-kS/s sampling rate and then undersampled at 0.1 kS/s.

Fig. 2 Workpiece, AISI 52100 alloy steel bar

A National Instrument DAQ board (NI 9232) was used for the digitization of all detected sensor signals. The sensor signals were stored as text files with a variable number of samplings per file according to the relative sampling rate of the diverse sensor signal types (Table 1). A total number of 5580 sensor signal files were obtained.

2.4 Surface roughness measurements

The typical apparatus employed for measuring surface roughness is a profilometer using a stylus that is drawn along the surface at constant speed measuring the vertical variation in surface smoothness variations [33].

After each polishing session, the process was halted, the workpiece dismounted, and surface roughness measured using a Mahr profilometer (MarSurf XR 1). The parameters of interest were R_a (average deviation), R_z (surface roughness based on the five highest peaks and lowest valleys over the entire sampling length), and R_t (total height) [32]. Five surface roughness measurements were done at the end of the polishing session, and the average of each of R_a, R_z, and R_t was calculated. The workpiece was then mounted again, and the polishing process was continued. The average values of the surface roughness parameters are reported in the graph in Fig. 4 and Table 2, and it can be noted that the final surface roughness, i.e., the surface roughness of the workpiece after the sixth session, was not measured.

3 Sensor signal processing and analysis

3.1 Acoustic emission sensor signals

The AE raw signals are expected to oscillate around the zero value providing a zero mean in time [34, 35]. As the detected AE signals presented a bias, possibly due to an electronic/electrical offset generated by the AE sensor system, a pre-processing step was carried out to remove the bias from the detected AE signals by shifting these signals so that a zero

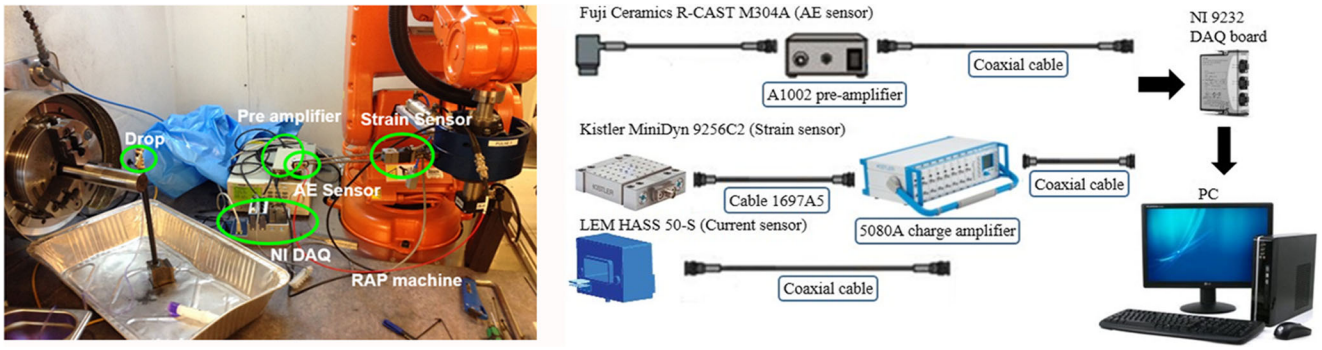

Fig. 3 Multiple sensor-monitoring system mounted on the RAP machine, AE sensor and pre-amplifier, strain sensor, and DAQ board. "Drop" indicates the utilized lubrication system [26]. The current sensor was mounted in the electrical cabinet of the machine

mean was obtained. The pre-processing procedure was carried out using MATLAB® by the following steps:

- Plotting of AE_{raw} signals (Fig. 5a)
- Shifting of AE_{raw} signals, for each AE_{raw} signal, the mean value was calculated and subtracted from each signal sampling to obtain the typical AE signal oscillating around zero (Fig. 5b)
- Moreover, for each unbiased AE_{raw} signal, the root-mean-square (RMS) with time constant 0.12 ms was calculated to obtain the corresponding AE_{RMS} signal (Fig. 5c) [35].

3.2 Strain and current sensor signals

A pre-processing phase was not required for the detected strain and current sensor signals. In Figs. 6 and 7, an example of strain and current sensor signal variation is reported for 1 s of polishing, respectively. The strain sensor signal was acquired at a sampling frequency of 50 kS/s and was undersampled to 16,384 samples per second. The strain samples, shown in Fig. 6, consist of a segment taken at an arbitrary moment from the 50,000 samples of the strain sensor signal corresponding to 1 s of polishing. The same was applied to the current sensor signals that were acquired at a sampling rate of 50 kS/s and then undersampled to 0.1 kS/s (Fig. 7).

Table 1 Sampling frequency and number of samplings (per file) for the three diverse sensing units

Sensor	Sensing variable	Sampling frequency	Number of samplings per file
Fuji Ceramics R-CAST M304A	AE	1 MHz undersampled at ~131 kS/s	131,072
Kistler MiniDyn 9256C2	Strain	50 kS/s undersampled at ~16 kS/s	16,384
LEM HASS 50-S	Current	50 kS/s undersampled at 0.1 kS/s	100

4 Sensor signal feature extraction

The following two types of feature extraction methods were used to process the digitized AE (AE_{raw} and AE_{RMS}), strain, and current sensor signals [26, 31]:

- Conventional feature extraction method
- Wavelet packet transform feature extraction method.

The extracted relevant features were subsequently used to construct different types of pattern feature vectors (simple and sensor fusion pattern vectors) to be fed to a neural network pattern recognition paradigm in order to make a decision on polished part surface roughness-level acceptability.

4.1 Conventional feature extraction method

The conventional feature extraction method consists of calculating statistical features from each of the AE, strain, and current sensor signals. These statistical features were mean (M), variance (V), skewness (S), kurtosis (K), and energy (E).

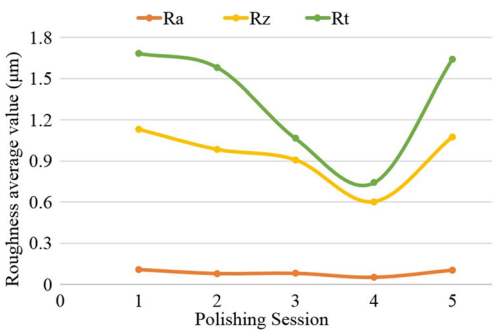

Fig. 4 Measured surface roughness parameters vs. polishing sessions

Table 2 Surface roughness measurements

Polishing session	Roughness average value (μm)		
	R_a	R_z	R_t
1 (60 passes with 1800 g)	0.111	1.131	1.684
2 (60 passes with 1000 g)	0.081	0.984	1.582
3 (60 passes with 1000 g)	0.083	0.908	1.065
4 (60 passes with 1000 g)	0.053	0.603	0.742
5 (60 passes with 1800 g)	0.107	1.076	1.643
6 (60 passes with 1800 g)	NA	NA	NA

Subsequently, two kinds of statistical pattern feature vectors (using features extracted from either AE_{raw} or AE_{EMS}) were constructed using the extracted statistical signal features.

4.2 Wavelet packet transform feature extraction method

The WPT of a signal decomposes the original signal into a number of packets of coefficients calculated by scaling and shifting a chosen mother wavelet that is a prototype function [31]. Accordingly, at the first level of WPT, the original sensor signal *S* is split into two frequency band packets, approximation A1 and detail D1. At the second level, each approximation and detail packet is again split into further approximations, AA2 and AD2, and details, DA2 and DD2, and the process is repeated generating other decomposition packets (Fig. 8) [36].

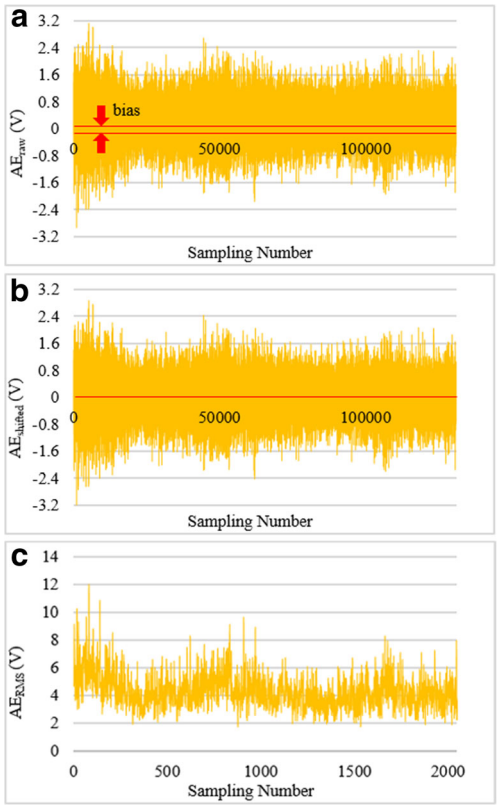

Fig. 5 **a** AE_{raw} signal, **b** AE_{raw}-shifted signal, and **c** AE_{RMS} signal

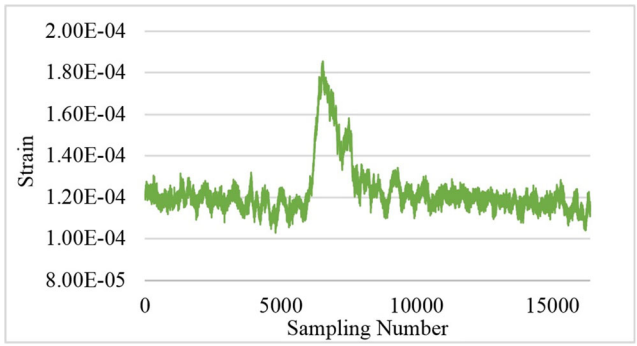

Fig. 6 Strain sensor signal

In this paper, the employed mother wavelet for the processing of the sensor signals is a Daubechies 3 (db3). The decomposition was performed up to the third level yielding 14 packets, 2 in the first level (A_1, D_1), 4 in the second level (AA_2, DA_2, AD_2, DD_2), and 8 in the third level (AAA_3, DAA_3, ADA_3, DDA_3, AAD_3, DAD_3, ADD_3, DDD_3) (Fig. 8). For each wavelet packet, the following five features were calculated: mean, variance, skewness, kurtosis, and energy.

To illustrate the WPT feature extraction procedure [27, 28], an example with reference to feature extraction from the sole wavelet packet A is reported in Fig. 9 and explained below.

The WPT algorithm was applied to the 5580 sensor signals resulting in the corresponding A packets consisting of a number of coefficients equal to half of the number of samplings of the original sensor signal files. For each A packet, five statistical packet features (mean, variance, kurtosis, skewness, energy) were calculated from its coefficients. The same procedure is repeated for the extraction of features from the other wavelet packets of the first, second, and third levels.

Overall, 14 packets × 2 AE signal types (AE_{raw} and AE_{RMS}) = 28 WPT pattern feature vectors were obtained.

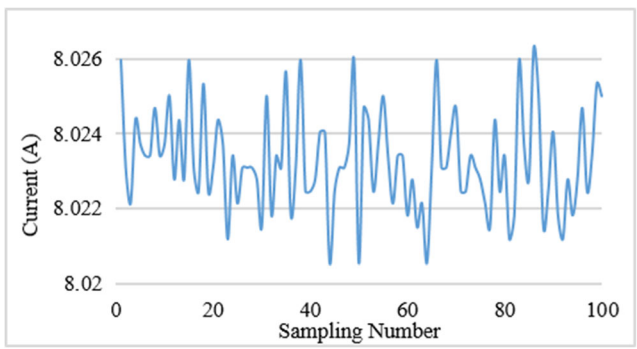

Fig. 7 Current sensor signal

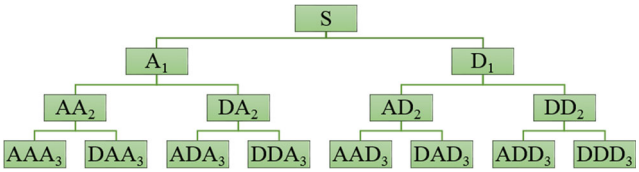

Fig. 8 Decomposition wavelet tree up to the third level. *S* original signal

5 Feature pattern vector construction

The extracted statistical and WPT features from the diverse sensor signals were utilized to construct the following two kinds of pattern feature vectors [37, 38]:

- Five-element pattern feature vectors, these vectors consist of the five features (statistical or WPT) extracted from each AE_{raw}, AE_{RMS}, strain, and current sensor signals. For example, the five-element pattern feature vectors, in the case of the extracted statistical (Stat) or WPT feature for AE_{raw}, are
- [Stat]AE_{raw} = [mean, variance, skewness, kurtosis, energy]AE_{raw}
- [WPT]AE_{raw} = [mean of wavelet packet, variance of wavelet packet, skewness of wavelet packet, kurtosis of wavelet packet, energy of wavelet packet]AE_{raw}.

Using the pattern feature vector scheme above, for AE_{raw}, 14 WPT 5-element pattern features vectors were constructed for each wavelet packet.

- Fifteen-element pattern feature vectors, a more complex vector combining the five features (statistical or WPT) extracted from each AE_{raw}/AE_{RMS}, strain, and current sensor signals for sensor fusion. For example, the 15-element sensor fusion (SF) pattern feature vectors, in the case of the extracted statistical (SFStat) or WPT (SFWPT) feature for AE_{raw}, are
- [SFStat]AE_{raw} = {[mean, variance, skewness, kurtosis, energy]AE_{raw}, [mean, variance, skewness, kurtosis, energy]strain, [mean, variance, skewness, kurtosis, energy]current}
- [SFWPT]AE_{raw} = {[mean of wavelet packet, variance of wavelet packet, skewness of wavelet packet, kurtosis of wavelet packet, energy of wavelet packet]AE_{raw}, [mean of wavelet packet, variance of wavelet packet, skewness of wavelet packet, kurtosis of wavelet packet, energy of wavelet packet]strain, [mean of wavelet packet, variance of wavelet packet, skewness of wavelet packet, kurtosis of wavelet packet, energy of wavelet packet]current}.

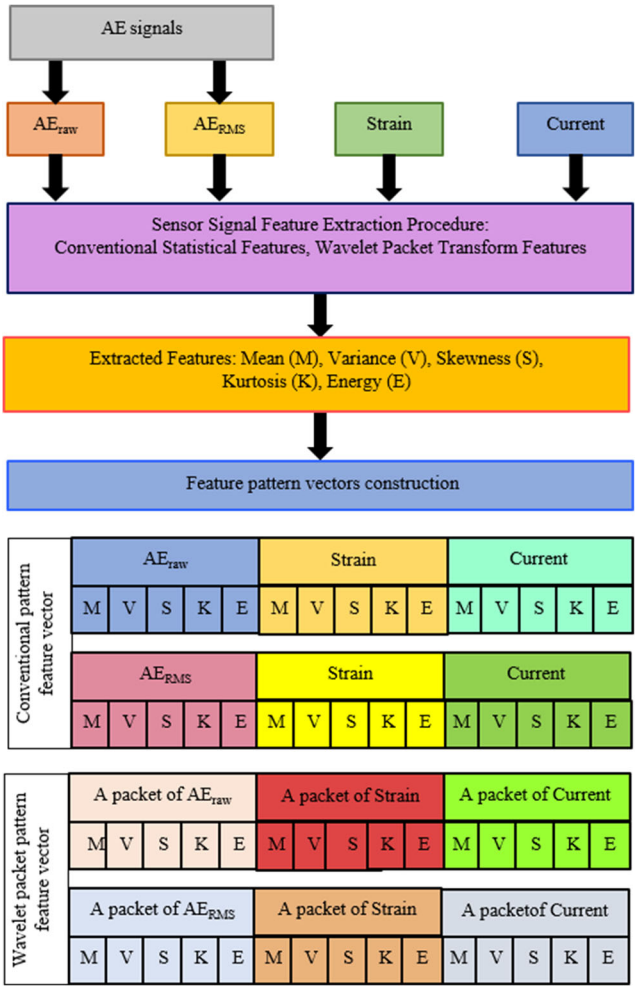

Fig. 10 Sensor signal feature extraction and feature pattern vector construction for both conventional statistical and wavelet packet transform methods from the following four diverse sensor signal types: AE_{raw}, AE_{RMS}, strain, and current

Using the pattern feature vector scheme described for AE_{raw}, 14 WPT 15-element pattern feature vectors are constructed for each wavelet packet.

Overall, in the case of the statistical feature vector extraction, 4 statistical 5-element pattern feature vectors ([Stat]AE_{raw}, [Stat]AE_{RMS}, [Stat]strain, [Stat]current) + 2 statistical 15-element sensor fusion pattern feature vectors ([SFStat]AE_{raw}, [SFStat]AE_{RMS}) were obtained.

As for the constructed WPT pattern feature vectors, 4 WPT 5-element pattern feature vectors ([WPT]AE_{raw},

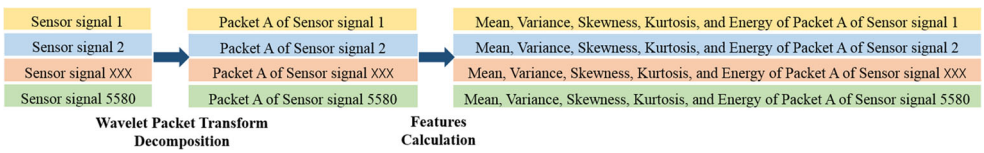

Fig. 9 WPT feature extraction method for the sole wavelet packet A

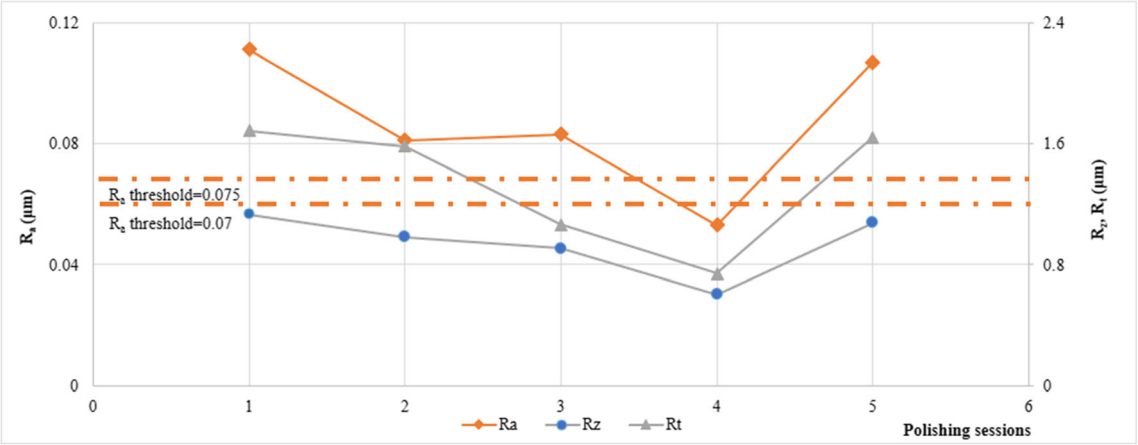

Fig. 11 The *broken straight lines* denote the measured roughness value graphs. The *horizontal dotted lines* denote the minimum and maximum R_a threshold levels

[WPT]AE_{RMS}, [WPT]strain, [WPT]current) + 2 WPT 15-element sensor fusion pattern feature vectors ([SFWPT]AE_{raw}, [SFWPT]AE_{RMS}) were constructed for each of the 14 packets.

A total number of 84 WPT pattern feature vectors were obtained. Figure 10 illustrates the sensor signal feature extraction and feature pattern vector construction for both conventional statistical and wavelet packet transform methods from the following four diverse sensor signal types: AE_{raw}, AE_{RMS}, strain, and current. The constructed feature pattern vectors were then utilized as input vectors to knowledge-based, decision-making paradigms.

6 Neural network pattern recognition

NN systems are inspired by the biological nervous system. They are computing systems made up of a number of simple, highly interconnected processing elements, called nodes, which perform in parallel processing information data by their dynamic state response to external inputs [39]. The connections between nodes determine the network function, and by adjusting the connection weights, NNs are trained to perform diverse specific functions. Among these, pattern recognition, i.e., identifying patterns in the input features relating them to the target output, is particularly effective for classification purposes [29].

Table 3 NN training set for the diverse threshold values, R_a = 0.070 μm and R_a = 0.075 μm

Threshold level (μm)	Acceptable roughness	Unacceptable roughness	NN binary code output value
R_a = 0.070 μm	2924	2656	0
R_a = 0.075 μm	3174	2406	1

6.1 Neural network design

The obtained statistical and WPT pattern feature vectors were employed as input to decision-making paradigms, based on NN pattern recognition, aimed at assessing the acceptability of the workpiece surface roughness during robot-assisted polishing.

In this work, NN implementation was carried out in MATLAB® environment using the Neural Network Toolbox [36]. The NN architecture is composed of the following three layers:

– Input layer
– Hidden layer(s)
– Output layer.

After several simulation trials, it was decided to have only one hidden layer and the number of nodes in the hidden layer to be equal to three times the numbers of nodes in the input layer. Data for pattern recognition and classification purposes were set up to be inputted to NN by organizing data into the following two matrices: input matrix and target matrix.

The input matrix is made of the 5- or 15-element feature vectors (columns) and the 5580 polishing test cases (row) corresponding to the 5580 acquired sensor signals.

The output layer (target matrix) had only one node, providing a binary target value associated with surface roughness acceptability, "0" for acceptable and "1" for unacceptable roughness.

Two different three-layer feed-forward (FF) back-propagation (BP) NN architectures [28] were implemented for each of the 90 input pattern feature vectors, 84 WPT pattern feature vectors plus 6 statistical pattern feature vectors by varying the number of input nodes and the number of hidden layer nodes depending on the number of input pattern vectors.

- Five-element input pattern feature vectors, in this case, the NN configuration is 5-15-1, where the 5-node input layer

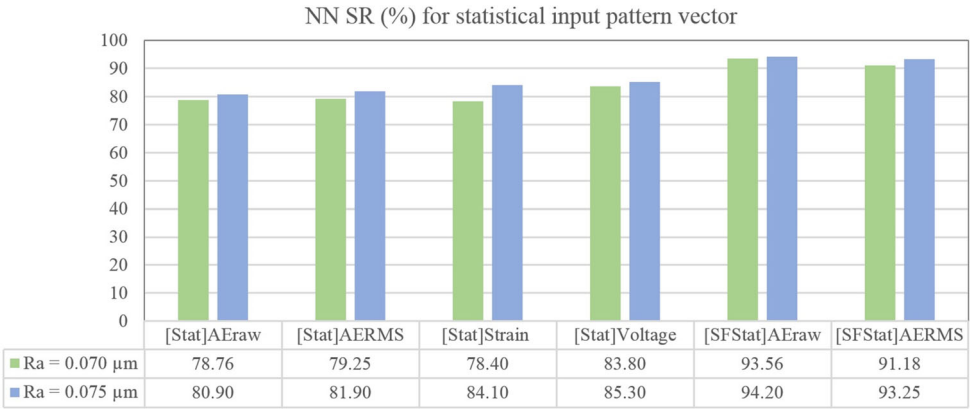

Fig. 12 Overall NN SR for all statistical input pattern feature vectors and the two threshold levels (R_a = 0.070 µm, R_a = 0.075 µm); [Stat]AE_{raw}, [Stat]AE_{RMS}, [Stat]strain, and [Stat]current are the five-element statistical input pattern feature vectors, and [SFStat]AE_{raw} and [SFStat]AE_{RMS} are the 15-element sensor fusion statistical input pattern feature vector

corresponded to the 5 features of each pattern vector and 15 nodes were utilized in the hidden layer

- Fifteen-element input pattern feature vectors, 15-45-1. The 15 nodes corresponded to the 15 features of each pattern vector, and the hidden layer was constituted of 45 nodes.

6.2 Neural network training and testing

The NN training set was constructed by associating the appropriate binary target value to each of the sensor signal files in order to map the input sensor signal pattern feature vectors to the output surface roughness acceptability. This was achieved as follows: the measured R_a values were linearly connected to form a broken line graph, and two threshold levels for surface roughness acceptability were selected (Fig. 11), representing the following two diverse target roughness values required from the polishing process: R_a = 0.070 µm and R_a = 0.075 µm. These threshold values were set according the industrial machining requirements. For each threshold level, sensor signal files corresponding to a linearly interpolated R_a value lower than or equal to the selected threshold were associated to a 0 binary output, i.e., acceptable roughness, and sensor signal files corresponding to a linearly interpolated R_a value higher than the selected threshold were associated to a 1 binary value, i.e., unacceptable roughness. The number of the acceptable and unacceptable cases is summarized in Table 3.

The NN training and testing procedure were carried out by sub-dividing the relevant training set, called sample, into the following three sub-sets: training sub-set (70 % of the sample instances), validation sub-set (15 % of sample instances), and testing sub-set (15 % of the sample instances). The output of

Table 4 Overall NN SR for all WPT input pattern feature vectors (threshold = 0.070)

Neural network SR (%)—threshold level, R_a = 0.070 µm						
Wavelet packet	WPT input pattern feature vector					
	[WPT]AE_{raw}	[WPT]AE_{RMS}	[WPT]strain	[WPT]current	[SFWPT]AE_{raw}	[SFWPT]AE_{RMS}
A	84.23	82.23	84.2	85.3	92.85	90.63
D	83.45	83.31	85.3	85.3	91.58	91.52
AA	84.98	81.13	84.7	85.4	91.23	92.45
DA	83.44	83.35	85.3	85	92.56	91.56
AD	81.89	82.82	84.7	85.3	93.85	90.75
DD	83.74	82.23	85	85.2	92.58	91.23
AAA	85.38	85.21	84.2	85.3	93.12	90.32
DAA	83.56	82.12	85.2	85.3	91.47	91.23
ADA	86.69	84.56	85.3	85.3	90.57	92.65
DDA	84.34	85.47	85.3	85.5	91.56	93.44
AAD	83.65	83.23	85.4	85.3	91.23	91.81
DAD	85.52	84.65	85.3	85.3	92.91	90.88
ADD	82.24	82.88	85.1	85.3	91.19	92.26
DDD	85.25	83.34	85.3	85.3	93.61	92.85
$SR_{average}$	84.16	83.32	85.02	85.29	92.16	91.79

Table 5 Overall NN SR for all WPT input pattern feature vectors (threshold = 0.075)

Neural network SR (%)—threshold level, R_a = 0.075 μm						
Wavelet packet	WPT input pattern feature vector					
	[WPT]AE_{raw}	[WPT]AE_{RMS}	[WPT]strain	[WPT]current	[SFWPT]AE_{raw}	[SFWPT]AE_{RMS}
A	85.5	83.2	86.4	92.8	95.5	95.5
D	85.3	84.7	88.6	86.6	95.3	96.1
AA	86.8	87.1	85.5	91.2	96.8	92.3
DA	85.4	85.2	88.2	87.7	95.4	95.5
AD	87.8	87.5	89	86.6	97.8	97.2
DD	88.1	87.1	87.1	87.1	98.1	96.2
AAA	87.3	86.5	85.5	88.2	97.3	94.8
DAA	87.2	87.8	88.6	86.5	97.2	95.2
ADA	85.8	86.2	88.7	86.6	95.8	94.7
DDA	86.2	88.2	88.6	86.2	96.2	94.3
AAD	86.8	85.7	88.3	86.6	96.8	95.2
DAD	87.5	87.9	88.5	86.6	97.5	95.6
ADD	84.2	83.3	88.3	86.6	94.2	95.8
DDD	84.8	85.4	85.9	86.6	94.8	93.2
$SR_{average}$	86.33	86.12	87.65	87.56	96.33	95.11

the NN pattern recognition paradigm consists of the following four percentage values, called success rates (SR): training set SR, validation set SR, testing set SR, and overall SR. The SR of interest to evaluate the NN performance in correctly assessing the acceptability of the workpiece surface roughness is the overall SR, the percentage of overall correct classifications that the NN has achieved in relating the input pattern feature vectors to the target surface roughness acceptability [39].

7 Results and discussion

In this section, the results of the NN pattern recognition paradigm in terms of NN SR (%) were reported for the two diverse input pattern feature vectors.

7.1 Statistical input pattern feature vectors

The overall NN SR for the statistical input pattern feature vectors is reported in Fig. 12. From the figure, it can be observed that, for both threshold values (R_a = 0.070 μm and R_a = 0.075 μm), the statistical pattern feature vectors provided interestingly high average SR value equal to 85.38 %. Moreover, the sensor fusion statistical pattern vectors ([SFStat]AE_{raw}, [SFStat]AE_{RMS}) shown a higher SR ranging from 91.18 to 94.20 % than the single statistical input pattern vectors ([Stat]AE_{raw}, [Stat]AE_{RMS}, [Stat]strain, [Stat]current) ranging from 78.40 to 85.30 %.

7.2 WPT input pattern feature vectors

In Tables 4 and 5, the overall NN SR values (%) were reported for the two threshold values (R_a = 0.070 μm and R_a = 0.075 μm) both in the case of the single WPT input pattern feature vectors and in the case of the WPT sensor fusion input pattern feature vectors for each of the 14 wavelet packets.

In the case of the threshold value R_a = 0.070 μm, the single WPT input pattern feature vectors ([WPT]AE_{raw}, [WPT]AE_{RMS}, [WPT]strain, [WPT]current) resulted in a NN SR ranging in the interval of 81.13–86.69 %, whereas for the sensor fusion WPT pattern vectors ([SFWPT]AE_{raw}, [SFWPT]AE_{RMS}), the NN SR varied from 90.32 to 93.85 %.

For the threshold value R_a = 0.075 μm, the NN SR for the single WPT input pattern feature vectors ([WPT]AE_{raw}, [WPT]AE_{RMS}, [WPT]strain, [WPT]current) varied from 83.2 to 92.8 %, whereas for the sensor fusion WPT pattern vectors ([SFWPT]AE_{raw}, [SFWPT]AE_{RMS}), the NN SR varied in the interval from 92.3 to 98.1 %.

As regards the behavior of the 14 wavelet packets, the following considerations can be done:

- Threshold value R_a = 0.070 μm, the wavelet packet AD was identified as that generating the most performing pattern feature vectors with NN SR > 93 % obtained for the sensor fusion pattern feature vector [SFWPT]AE_{raw}
- Threshold value R_a = 0.075 μm, the wavelet packet DD is the most performing pattern feature vectors with NN

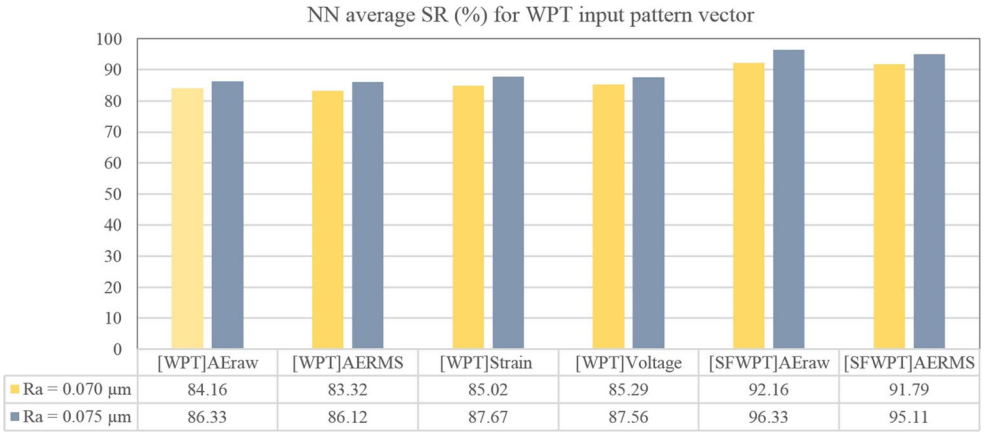

Fig. 13 Overall average of NN SR for all WPT input pattern feature vectors and the two threshold levels (R_a = 0.070 μm, R_a = 0.075 μm); [WPT]AE_{raw}, [WPT]AE_{RMS}, [WPT]strain, and [WPT]current are the 5-element WPT input pattern feature vectors, and [SFWPT]AE_{raw} and [SFWPT]AE_{RMS} are the 15-element sensor fusion WPT input pattern feature vector

SR > 98 % achieved in the case of the sensor fusion pattern feature vector [SFWPT]AE_{raw}.

In Fig. 13, the overall average NN SR is reported for all WPT input pattern feature vectors and for the two threshold levels. The NN SR values reported in the figure correspond to the last row of Tables 4 and 5.

7.3 Comparison

By comparing Figs. 12 and 13, it can be noticed that, for both threshold levels, the NN SR values achieved for the sensor fusion pattern feature vectors are always higher than for any of the statistical and WPT pattern feature vectors, especially for the AE_{raw} signal. This confirms the high efficacy of sensor fusion technique in making full use of sensorial information. Furthermore, the increase of threshold value augments the NN SR in assessing the surface roughness acceptability. This can be explained by the higher number of acceptable roughness cases generated by the higher threshold that ensures a more balanced NN training set and, hence, a better NN performance. However, threshold increase should be treated with care as too high a value may unbalance the NN training set in the opposite way and, what is more, may fail to agree with the polishing process quality requirements.

8 Conclusions

In this paper, a multiple sensor-monitoring system was installed on a robot-assisted polishing machine in order to enhance the automated polishing operations in terms of surface roughness quality acceptability.

To achieve this goal, the previously analyzed sensor signals (AE (AE_{raw} and AE_{RMS}), strain, and current) were subjected to the following two feature extraction techniques: a conventional one based on statistical analysis and an advanced one based on wavelet packet transform. Furthermore, workpiece surface roughness (R_a, R_z, R_t) was measured after each polishing session, and two diverse threshold levels for surface roughness acceptability were selected (R_a = 0.070 μm and R_a = 0.075 μm), representing two diverse target roughness values required from the polishing process according the industrial machining requirements.

The extracted statistical and WPT features were utilized to construct the following two kinds of pattern feature vectors: 5-element pattern feature vectors and more complex 15-element sensor fusion pattern feature vectors combining the information from the diverse sensor signals. The obtained 90 input pattern feature vectors (84 WPT pattern feature vectors plus 6 statistical pattern feature vectors) were fed to NN-based pattern recognition paradigms for decision making on polished workpiece surface roughness acceptability. By comparing the results obtained with the conventional and the advanced WPT feature extraction methods for both threshold values, the NN performance for the WPT pattern feature vectors (average SR = 86.94 % for R_a = 0.070 μm; average SR = 89.85 % for R_a = 0.075 μm) was higher than the one of the statistical pattern feature vectors (average SR = 84.16 % for R_a = 0.070 μm; average SR = 86.61 % for R_a = 0.075 μm), asserting the effectiveness of the WPT signal analysis methodology for sensor monitoring of material removal processes.

The higher NN SR was always obtained when the sensor fusion pattern vectors were considered, always >90 %. This was due to the fact that the sensor fusion pattern vectors that combined the information of all diverse sensing units utilized in the experimental tests allow to achieve a more suitable data set for pattern recognition decision-making support system.

The proposed procedure based on a multiple sensor-monitoring system together with advanced sensor signal-processing procedure and cognitive decision-making paradigm is suitable for online process control of the RAP machine in terms of surface roughness assessment, and thus, a complete automation of polishing process characterized by high robustness, reliability, reconfigurability, and intelligence can be implemented.

Acknowledgments This research work has received funding support from the EC FP7 under grant agreement no. 285489—Intelligent Fault Correction and self-Optimizing Manufacturing systems (IFaCOM). The Fraunhofer Joint Laboratory of Excellence for Advanced Production Technology (Fh-J_LEAPT) at the Department of Chemical, Materials and Industrial Production Engineering, University of Naples Federico II, is gratefully acknowledged for its support to this work.

References

1. Evans CJ, Paul E, Dornfeld D, Lucca DA, Byrne G, Tricard M, Klocke F, Dambon O, Mullany BA (2003) Material removal mechanisms in lapping and polishing. CIRP Ann 52(2):611–633
2. Marinescu I, Uhlmann E, Doi T (2006) Handbook of lapping and polishing. CRC Press, Taylor & Francis Group
3. Komanduri R, Lucca DA, Tani Y (1997) Technological advances in fine abrasive processes. CIRP Ann 46(2):545–596
4. Rebeggiani S, Rosén B G (2011) High gloss polishing of tool steels—step by step. Proc. of the 4th Swedish Production Symposium, Lund, Sweden. The Swedish Production Academy, pp 257–262
5. Eriksen RS, Arentoft M, Grønbæk J, Bay N (2012) Manufacture of functional surfaces through combined application of tool manufacturing processes and robot assisted polishing. CIRP Ann 61(1):563–566
6. Klocke F, Dambon O, Behrens B (2011) Analysis of defect mechanisms in polishing of tool steels. Production Engineering—Research and Development 5(5):475–483
7. Byrne G, Dornfeld D, Inasaki I, König W, Teti R (1995) Tool condition monitoring (TCM)—the status of research and industrial application. CIRP Ann 44(2):541–567
8. Wang C, Ghani SBC, Cheng K, Rawkoski R (2013) Adaptive smart machining based on using constant cutting force and a smart cutting tool. Proc of the IMechE, Part B: Journal of Engineering Manufacture 227(2):249–253
9. Wang C, Cheng K, Chen X, Minton T, Rawkoski R (2014) Design of an instrumented smart cutting tool and its implementation and application perspectives. Smart Mater Struct 23(3):350–362
10. Jemielniak K, Teti R, Kossakowska J, Segreto T (2006) Innovative signal processing for cutting force based chip form prediction. In: Intelligent Production Machines and Systems—2nd I*PROMS Virtual International Conference, pp 7–12
11. Micheletti GF, Koenig W, Victor HR (1976) In process tool wear sensors for cutting operations. CIRP Ann 25(2):483–496
12. Toenshoff HK, Wulfsberg JP, Kals HJJ, van Luttervelt CA (1988) Development and trends in monitoring and control of machining processes. CIRP Ann 37(2):611–622
13. Teti R, Jemielniak K, O'Donnell G, Dornfeld D (2010) Advanced monitoring of machining operations. CIRP Ann 59(2):717–739
14. Klein LA (2004) Sensor and data fusion: a tool for information assessment and decision making. SPIE Press Book
15. Hall D, Llinas J (2001) Handbook of multisensor data fusion. CRC Press
16. White FE (1991) Data fusion lexicon, joint directors of laboratories, technical panel for C3, data fusion sub-panel. Naval Ocean Systems Center, San Diego
17. Ghosh N, Ravi A, Patra S, Mukhopadhyay S, Mohanty A, Chattopadhyay A (2007) Estimation of tool wear during CNC milling using NN-based sensor fusion. Mech Syst & Sign Proc 21:466–479
18. Chen L, Bender P, Renton P, El-Wardany T (2002) Integrated virtual manufacturing systems for process optimisation and monitoring. CIRP Ann 51(1):409–412
19. Huang B, Chen JC (2003) An in-process neural network-based surface roughness prediction system using a dynamometer in end milling operations. Int J Adv Manuf Technol 21:339–347
20. Binsaeid S, Asfoura S, Chob S, Onarc A (2009) Machine ensemble approach for simultaneous detection of transient and gradual anomalies in milling using multisensor fusion. J. Mat Proc Techn 209: 4728–4738
21. Ahn JH, Shen YF, Kim HY, Jeong HD, Cho KK (2001) Development of a sensor information integrated expert system for optimizing die polishing. Robot Comput Integr Manuf 17:269–276
22. Ahn JH, Lee MC, Jeong HD, Kim SR, Cho KK (2002) Intelligently automated polishing for high quality surface formation of sculptured die. J Mater Process Technol 130-131:339–344
23. Lee DE, Hwang I, Valente CMO, Oliveira JFG, Dornfeld DA (2006) Precision manufacturing process monitoring with acoustic emission. Int J Adv Manuf Technol 46:176–188
24. Chang YP, Hashimura M, Dornfeld DA (1996) An investigation of the AE signals in the lapping process. CIRP Ann 45:331–334
25. Dunegan H (1998) An acoustic emission technique for measuring surface roughness. The DECI report. Dunegan Engineering Consultants Inc., Midland, Texas 79711
26. Segreto T, Karam S, Teti R, Ramsing J (2015) Cognitive decision making in multiple sensor monitoring of robot assisted polishing. Procedia CIRP 33:333–338
27. Karam S, Teti R (2013) Wavelet transform feature extraction for chip form recognition during carbon steel turning. Procedia CIRP 12:97–102
28. Segreto T, Karam S, Simeone A, Teti R (2013) Residual stress assessment in Inconel 718 machining through wavelet sensor signal analysis and sensor fusion pattern recognition. Procedia CIRP 9: 103–108
29. Bishop CM (1995) Neural networks for pattern recognition. Clarendon Press, Oxford
30. Segreto T, Simeone A, Teti R (2014) Principal component analysis for feature extraction and NN pattern recognition in sensor monitoring of chip form during turning. CIRP J of Manuf Sci and Techn 7:202–209
31. Segreto T, Karam S, Teti R, Ramsing J (2015) Feature extraction and pattern recognition in acoustic emission monitoring of robot assisted polishing. Procedia CIRP 28:22–27
32. EC FP7, call for FoF, towards zero-defect manufacturing, 2011-NMT-ICT-FoF, intelligent fault correction and self optimising manufacturing systems—IFaCOM (2011–15)
33. (2011) Exploring surface texture: a fundamental guide to the measurement of surface finish, 7th ed. Taylor Hobson, UK
34. Beattie AG (1979) Studies in the digital analysis of acoustic emission signals. In: Kanji Ono (ed) Fundamentals of acoustic emission. University of California LA, pp 17–47
35. Webster J, Dong WP, Lindsay R (1996) Raw acoustic emission signal analysis of grinding process. CIRP Ann 45(1):335–340
36. Misiti M, Misiti Y, Oppenheim G, Poggi JM (1997-2014) Wavelet toolbox for use with MATLAB. The MathWorks, Inc
37. Segreto T, Simeone A, Teti R (2013) Multiple sensor monitoring in nickel alloy turning for tool wear assessment via sensor fusion. Procedia CIRP 12:85–90
38. Segreto T, Simeone A, Teti R (2012) Sensor fusion for tool state classification in nickel superalloy high performance cutting. Procedia CIRP 1:593–598
39. Jordan MI, Bishop CM (2004) Neural networks. In: Allen B. Tucker (edn) Computer science handbook, 2nd edn. (Section VII: Intelligent Systems), Chapman & Hall/CRC Press LLC